

# Electron concentration effects on the Shastry-Sutherland phase stability in $\text{Ce}_{2-x}\text{Pd}_{2+y}\text{In}_{1-z}$ solid solutions

J.G. Sereni<sup>1</sup>, M. Giovannini<sup>2</sup>, M. Gómez Berisso<sup>1</sup>, A. Saccone<sup>2</sup>

<sup>1</sup>*Div. Bajas Temperaturas, Centro Atómico Bariloche (CNEA) and Conicet, 8400 S.C. Bariloche, Argentina*  
<sup>2</sup>*CNR-SPIN, Dipartimento di Chimica e Chimica Industriale, Università di Genova, I-16146 Genova, Italy*

(Dated: September 29, 2010)

The stability of a Shastry-Sutherland ShSu phase as a function of electron concentration is investigated through the field dependence of thermal and magnetic properties of the solid solution  $\text{Ce}_{2-x}\text{Pd}_{2+y}\text{In}_{1-z}$  in the antiferromagnetic branch. In these alloys the electronic (holes) variation is realized by increasing *Pd* concentration. The AF transition  $T_M$  decreases from 3.5 K to 2.8 K as *Pd* concentration increases from  $y = 0.2$  to  $y = 0.4$ . By applying magnetic field, the ShSu phase is suppressed once the field induced ferromagnetic polarization takes over at a critical field  $B_{cr}$  which increases with *Pd* content. A detailed analysis around the critical point reveals a structure in the maximum of the  $\partial M/\partial B$  derivative, which is related with incipient steps in the magnetization  $M(B)$  as predicted by the theory for the ShSu lattice. The crossing of  $M(B)$  isotherms, observed in ShSu prototype compounds, is also analyzed. The effect of *In* substitution by *Pd* is interpreted as an increase of the number of 'holes' in the conduction band and results in a unique parameter able to describe the variation of the magnetic properties along the studied range of concentration.

PACS numbers: 71.20.LP; 74.25.Ha; 75.30.Mb

## I. INTRODUCTION

Magnetic frustration is an attracting topic of physics since it may drive the systems to new and exotic phases [1]. Frustration is mostly originated in peculiar geometrical conditions which impede the development of long range order. One of the simplest examples of magnetic frustration is a triangular coordination of moments interacting antiferromagnetically AF among them. Since a canonical AF minimum of energy cannot be reached, the system accesses to alternative minima where other types of order parameters may develop.

In the presence of AF interactions, Shastry-Sutherland ShSu lattices [2] present those characteristics because neighboring magnetic atoms are disposed in triangular arrangements. In the model compound  $\text{SrCu}_2(\text{BO}_3)_2$  [3], magnetic  $\text{Cu}^{2+}$  atoms have one nearest-neighbor *nn* and four next-nearest-neighbors *nnn* on the same plane, all of them coupled AF by respective  $J$  and  $J'$  exchanges. Since the effective interactions are  $J > J'$ , *nn* atoms form a network of  $J$  mediated orthogonal dimers, being the interaction between dimers mediated by  $J'$ . As a result, the magnetic structure can be described as a quasi 2D lattice of orthogonal dimers [4].

Two significant features were observed in the field  $B$  dependent magnetization  $M$  curves of  $\text{SrCu}_2(\text{BO}_3)_2$  [3]: i) a crossing of the magnetization isotherms at low temperature ( $T < 4$  K) and ii) two small steps in  $M(B)$  at fractional values (c.f. 1/4 and 1/8) of the saturation moment  $M_{sat}$ . In this compound, those steps are observed at a quite high applied magnetic field  $B \approx 20$  T [3]. This so-called 'quantized magnetization' scenario, with  $M=1/2, 1/4, 1/8, \dots$  of  $M_{sat}$  is explained by the theory [4] as due to successive commensurate shells of 2D squares involving integer number of dimers. This model considers the geometrical distribution of the magnetic en-

ties (i.e. dimers) as topologically equivalent to the 2D square lattice of the Heisenberg model. A simple series expansion according to  $N = 2^n$ , where  $n$  is an integer number  $n = 1, 2, \dots$ , accounts for the amount of dimers  $N$  involved in the successive shells as the magnetic field increases. As a consequence of the  $J$ -AF character, the four fold state of the dimers splits into a singlet ground state GS and an excited triplet [4].

Among intermetallic compounds, some heavy rare earth tetraborides  $\text{RB}_4$  [5] were found to show these features but at lower magnetic field, e.g. 4T for  $\text{ErB}_4$ , with a clear step at  $1/2M_{sat}$ . Similar scenario was invoked in  $\text{Yb}_2\text{Pt}_2\text{Pb}$  [6] which orders AF at  $T_M \approx 2$  K. Within the  $\text{Mo}_2\text{B}_2\text{Fe}$  type structure there is a large family of compounds with the formula  $\text{R}_2\text{T}_2\text{X}$ , being T a transition metal and X a p-metal. In this structure, the magnetic atoms 'R' are disposed in a unique crystalline lattice. Particularly, those compounds with  $T = \text{Pd}$  and  $X = \text{Sn}$  [7] or  $\text{In}$  [8] are of interest concerning the ShSu phase formation because of the triangular coordination of the 'R' magnetic atoms. This quasi 2D structure can be described as successive 'T+X' (at  $z = 0$ ) and 'R' (at  $z = 1/2$ ) layers [9], with the 'R' *nn* and *nnn* disposed with the same symmetry like in  $\text{SrCu}_2(\text{BO}_3)_2$ , albeit at different relative distances.

A ShSu phase was also reported in  $\text{Ce}_2\text{Pd}_2\text{Sn}$  [10] within a limited range of temperature, i.e. between an AF transition at  $T_M = 4.9$  K and a ferromagnetic FM one of first order type at  $T_C = 2.1$  K. Since in this compound dimer's formation is mediated by a  $J$ -FM exchange, the previously mentioned triplet has the lowest energy. The ShSu phase is built by a  $J'$ -AF exchange below  $T_M = 4.9$  K, however it becomes instable below  $T_C = 2.1$  K when the interplane FM interaction  $J_C$  takes over inducing a 3D-FM ground state GS.

The ShSu phase is suppressed under a relatively low

magnetic field at a magnetic critical point:  $B_{cr} = 0.11$  T and  $T_{cr} = 4.1$  K [11]. Despite of the low  $B_{cr}$  value, isothermal  $M(B)$  measurements show the features observed in the mentioned ShSu model compounds, i.e. the crossing of magnetization isotherms and an incipient step as a function of field at  $M \approx 1/4 M_{sat}$ .

The stability of the ShSu phase was also investigated under structural pressure, by doping  $Pd$  with smaller iso-electronic  $Ni$  atoms. The expected weakening of the Ce magnetic moment and the increase of the Sommerfeld coefficient  $\gamma$  occurs in  $Ce_2(Pd_{1-x}Ni_x)_2Sn$  as the Kondo screening increases. The upper transition temperature  $T_M(Ni)$  decreases due to the weakening of the  $J$  exchange [12]. On the contrary, the lower transition  $T_C$  to the FM phase increases with  $x(Ni)$  as a consequence of the reduction of the temperature range of the ShSu stability because of the weakening of the  $J'$  coupling. Both  $J$  and  $J'$  are overcome by the inter-Ce planes coupling in the 'c' crystalline direction  $J_C$ , which for  $x = 0.25$  practically inhibits the ShSu phase formation.

Besides magnetic field and structural pressure, the third complementary control parameter to be used to investigate this ShSu phase stability is the chemical potential variation. In this family of compounds, the significant range of solubility of the 2-2-1 ternary indides [13] provides the possibility to investigate the effect of the electronic concentration. Particularly, within the region where  $In$  sites can be occupied by  $Pd$  atoms, the number of 'holes' in the conduction band is expected to increase driven by  $Pd$  concentration. For such a purpose, we have performed a systematic study of the low temperature magnetic properties of  $Ce_{2-x}Pd_{2+y}In_{1-z}$  alloys within a broad range of composition.

## II. EXPERIMENTAL DETAILS AND RESULTS

The metals used for sample preparation were palladium (foil, 99.95 mass % purity, Chimet, Arezzo, Italy), cerium (bar, 99.99 mass % purity, NewMet Kock, Waltham Abey, UK) and indium (ingot, 99.999 % mass, Johnson Matthey, London, UK). The samples, each with a total weight of about 2 g, were prepared by weighing the proper amounts of elements and then by argon arc melting the elements on a water cooled copper hearth with a tungsten electrode. To ensure good homogeneity the buttons were turned over and remelted several times. Weight losses after melting were always smaller than 0.5 mass %. All the samples were then annealed at 750 C for 10 days, and finally quenched in cold water. Scanning electron microscopy SEM supplied by Carl Zeiss SMT Ltd. Cambridge, England, and electron probe micro-analysis EPMA based on energy-dispersive X-ray spectroscopy were used to examine phase compositions. Smooth surfaces of specimens for microscopic observation were prepared by using SiC papers and diamond pastes down to  $1 \mu$  grain size. The compositional contrast was revealed in un-etched samples by means of a backscat-

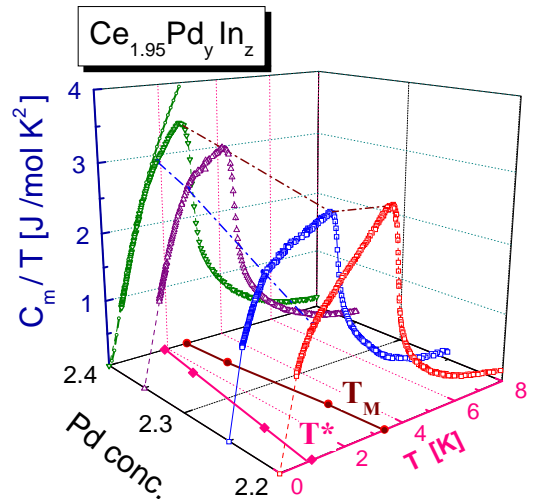


FIG. 1: (Color online) Thermal dependence of the magnetic contribution to specific heat  $C_m$  divided  $T$  for different  $Pd$  concentrations. Dash-dot curves are guides to the eye indicating  $T_M$  and  $T^*$  variations, which are also projected on the basal plane. Continuous curve on the  $Ce_{1.95}Pd_{2.4}In_{0.7}$  compound is the fit for  $T \leq T^*$ , see the text.

tered electron detector BSE. For the quantitative analysis an acceleration voltage of 20 KV was applied for 100 s, and a cobalt standard was used for calibration. The X-ray intensities were corrected for ZAF effects using the pure elements as standards. The composition values derived were usually accurate to 1 at%. X-ray diffraction XRD was performed on powder samples using the vertical diffractometer X-Pert MPD (Philips, Almelo The Netherlands) with Cu K radiation.

Specific heat was measured using a standard heat pulse technique in a semi-adiabatic He-3 calorimeter in the range between 0.5 and 20K, at zero and applied magnetic field up to 2T. DC-magnetization measurements were carried out using a standard SQUID magnetometer operating between 2 and 300K, and as a function of field up to 5T. For AC-susceptibility measurements a lock-in amplifier was used operating at 1.28KHz, with an excitation field of 10Oe on compensated secondary coils in the range of 0.5 to 10K.

The  $Ce_2Pd_2In$  system presents a wide range of solid solution [13], with a gap of solubility around the stoichiometric composition. Such a gap splits the range of solubility into two 'branches' which show distinct magnetic structures, being the Ce-rich branch FM and the Pd-rich one AF [13]. The studied alloys can be described by the general formula  $Ce_{2-x}Pd_{2+y}In_{1-z}$ , with:  $-0.1 \leq x \leq 0.1$ ,  $y = x + z$  and  $0.05 \leq z \leq 0.3$ , with the richest  $Pd$  composition placed at the edge of the chemical stability. Most of the work was performed on the AF-branch, but one alloy of the FM-branch (c.f.

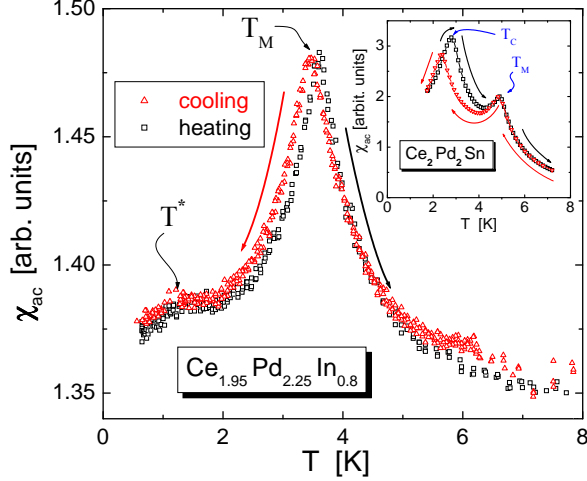


FIG. 2: (Color online) Low temperature ac-susceptibility of  $\text{Ce}_{1.95}\text{Pd}_{2.25}\text{In}_{0.8}$ . Inset: comparison with  $\text{Ce}_2\text{Pd}_2\text{Sn}$  after Ref.[10].

$\text{Ce}_{2.1}\text{Pd}_{1.95}\text{In}_{0.95}$ ) was also investigated for comparison with the aim to extend the study of the electron concentration effect.

Concerning the structural consequences of the  $\text{Pd}/\text{In}$  substitution in the alloys belonging to the  $\text{Pd}$ -rich AF-branch, one can recognize from the compositional dependence of the lattice parameters that the volume cell practically does not change. There is, however, a slight decrease of the 'a' lattice parameter accompanied by an increase of the 'c' parameter, which produces an increase of the 'c/a' ratio. Such a variation is explained by the fact that the excess of  $\text{Pd}$  replacing larger  $\text{In}$  atoms occupies two  $4e$  sites which lie on the 'c' axis symmetrically placed respect to the original  $\text{In} - 2a$  site [13]. As a consequence the Ce-Ce inter-planes distance is expected to increase with  $\text{Pd}$  content.

### 1. Thermal Properties

In Fig. 1 we compare the thermal dependence of the magnetic contribution to the specific heat for samples with concentration  $\text{Pd}(2+y) = 2.20, 2.25, 2.35$  and  $2.40$ , all of them belonging to the  $\text{Pd}$ -rich AF 'branch'. The magnetic contribution  $C_m(T)$  is computed by subtracting the  $C_P(T)$  of the non-magnetic isotypic La compound to the measured value. In the figure one can see that the transition  $T_M$  decreases upon increasing  $\text{Pd}$  concentration from  $3.5$  to  $2.8$  K (see the  $T_M$  projection on the basal plane). The maximum value of  $C_m/T_M$  first decreases between  $\text{Pd}(2+y) = 2.20$  and  $2.25$ , and then increases monotonously up to  $\text{Pd}(2+y) = 2.40$ . This non monotonous behavior can be attributed to different competing contributions which change differently with  $\text{Pd}$

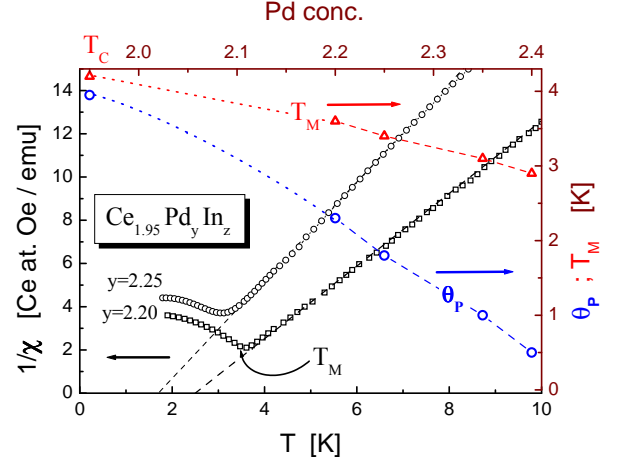


FIG. 3: (Color online) Low temperature inverse susceptibility ( $B/M$ , with  $B = 0.3T$ ) of two samples showing the paramagnetic temperature extrapolation  $\theta_P$  (left and lower axes).  $\text{Pd}$  concentration dependence of  $\theta_P$  and susceptibility cusp at  $T = T_M$  (right and upper axes), including the FM sample. Dot lines are the extrapolations of  $\theta_P$  and  $T_M$  parameters from AF samples (dashed lines) to those of the FM one.

content. The  $C_m(T_M)$  transition of the  $\text{Pd}(2+y) = 2.20$  shows a sharper and higher maximum than the other alloys, probably due to its lower disorder due to its proximity to stoichiometry. For higher  $\text{Pd}$  concentration, the maximum increases because of the  $C_m(T_M)$  ratio with decreasing  $T_M(\text{Pd})$  values.

Contrary to  $\text{Ce}_2\text{Pd}_2\text{Sn}$ , below  $T_M$  there is no first order transition (like  $T_C$ ), but a shoulder at a temperature  $T = T^*$  which increases with  $\text{Pd}$  content. Such a temperature is traced as the maximum curvature of  $C_m(T)/T$ . This weak change in the thermal dependence of  $C_m/T$  indicates that around that temperature the modulated phase [13] continuously transforms into the FM GS.

In order to check this difference between indides and stanides compounds, we have measured the ac-susceptibility  $\chi_{ac}$  on the  $\text{Pd}(2+y) = 2.25$  alloy, see Fig. 2. The  $\chi_{ac}(T)$  maximum at  $T = 3.6$  K coincides with the corresponding  $T_M$  value, but only a weak shoulder is detected at  $T = 1.5$  K in coincidence with  $C_m(T)/T$ . This temperature dependence has to be compared with that of  $\text{Ce}_2\text{Pd}_2\text{Sn}$  [10] shown in the inset. There, the first order character of the lower transition is clearly evidenced by the thermal hysteresis around  $T_C$ . On the contrary, the low signal and the lack of thermal hysteresis at  $T^*$  in the indide compound indicates that no magnetic transition occurs at that temperature.

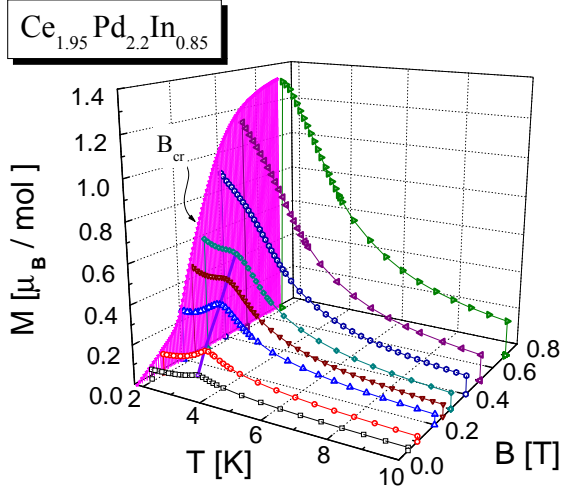


FIG. 4: (Color online) Thermal dependence of the magnetic isopedias for different applied fields. At  $T = 1.8$  K a  $M(B)$  is included and the continuous line at  $T \approx 3$  K connect the  $M(T_M)$  cusps.  $B_{cr}$  indicate the critical field at which the  $T_M$  transition vanishes.

## 2. Magnetic properties

The  $T_M(Pd)$  dependence was also traced by  $M(T)$  measurements. In Fig. 3 we show the inverse of the low temperature susceptibility measured with  $B = 0.3$  T on two representative samples:  $Ce_{1.95}Pd_{2.2}In_{0.85}$  and  $Ce_{1.95}Pd_{2.25}In_{0.8}$ . The respective paramagnetic temperatures  $\theta_P$  and AF transitions  $T_M$  are depicted in Fig. 3 as a function of  $Pd$  concentration (right and upper axes) for all studied alloys, including a FM one with  $Pd(2+y) = 1.95$ . One can see that  $\theta_P(Pd)$  rapidly decrease with  $Pd$  content, extrapolating to zero for  $Pd(2+y) \approx 2.43$ , whereas  $T_M(Pd)$  decreases moderately.

The measurement performed up to room temperature on the  $Ce_{1.95}Pd_{2.20}In_{0.85}$  sample (not shown) allowed to evaluate the magnetic moments of the ground and excited crystal field CF levels, and their respective CF splitting. For such a purpose we have used the simplified formula [14]:

$$M/B = \sum_{i=0}^2 \mu_i^2 * \exp(-\Delta_i/T) / [(T - T_I) * Z] \quad (1)$$

where  $\mu_i$  are the effective moments of the ground state ( $i=0$ ) and excited CF levels ( $i=1, 2$  respectively). The values obtained for the ground and first CF excited levels:  $\mu_0 = 1.6\mu_B$  and  $\mu_1 = 2.4 \pm 0.2\mu_B$ , with a CF splitting:  $\Delta_1 = 60 \pm 5$  K. These values are very similar to those obtained for  $Ce_2Pd_2Sn$  [10] and guarantee that only the GS doublet is responsible for the low temperature prop-

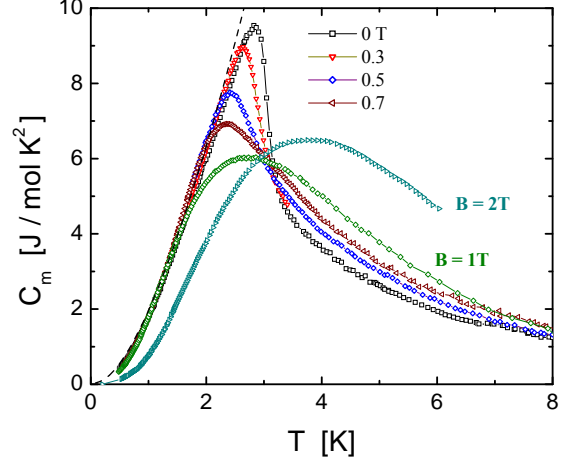


FIG. 5: (Color online) Magnetic field effect on the specific heat of  $Ce_{1.9}Pd_{2.4}In_{0.7}$  up to  $B = 2$  T. Dashed curve is the fit with for  $B = 0$  using eq.(2).

erties. As a consequence of the good fit obtained by applying eq(1) without including any *4f-conduction band* hybridization effect, one conclude that this system can be considered as formed by  $Ce^{3+}$  ions lattice with irrelevant Kondo effect (i.e.  $T_K < T_M$ ).

## 3. Field dependencies

The temperature dependence of magnetization  $M(T)$  was studied in all the samples under different applied fields up to  $B = 0.7$  T in order to obtain the respective magnetic phase diagrams. In Fig. 4 we present a detailed investigation performed on the  $Ce_{1.95}Pd_{2.20}In_{0.85}$  alloy, selected for having the composition closer to stoichiometry. Albeit those  $M(T)$  isopedias were measured between  $1.8 \leq T \leq 20$  K, they are only shown up to 10 K for clarity. The  $M(B)$  isotherm obtained at our lowest measured temperature ( $T = 1.8$  K) is also included in the  $M - B$  plane. These  $M(T)$  curves show an AF type behavior up to about  $B = 0.18$  T, turning into a field induced FM polarization at higher field. As this polarization arises, it overcome the  $T_M$  transition defined as the cusp of  $M(T)$  (see the continuous curve around  $T = 3$  K in Fig. 4). This indicates that the ShSu phase is suppressed at a critical field  $B_{cr}$  slightly above  $B = 0.3$  T. Notably,  $T_M$  itself is slightly affected by magnetic field because in that alloy it decreases from 3.56 K at 50 mT to 3 K at 0.3 T. This indicates that the intensity of the  $J$  and  $J'$  couplings are weakly affected by field despite of the degrees of freedom progressively transferred to the FM phase. This field dependence for all the studied alloys is included in the magnetic phase diagrams presented at the end of the discussion section.

The magnetic field effect on the specific heat  $C_m(T)$  was also studied in all the samples, however more detailed measurements were carried on the richest *Pd* sample  $\text{Ce}_{1.9}\text{Pd}_{2.4}\text{In}_{0.7}$ , up to  $B = 2\text{ T}$  as shown in Fig. 5. Since this alloy lies at the edge of the solid solution formation, we have chosen it for the field effect investigation in order to drive  $T_M$  to lower temperature and to trace the disappearance of the  $T^*$  shoulder. The temperature of the  $C_m(T)$  maximum (coincident with  $T_M$  defined by the cusp in  $M(T)$ ) progressively decreases with field till it reaches the value of  $T^*$  at  $B_{cr} = 0.7\text{ T}$ . Beyond that value the  $C_m(T)$  maximum broadens and start to increase in temperature with a typical behavior of a FM field-polarized system. Coincidentally, the  $C_m(T_M)$  jump is overcome by the high temperature tail of  $C_m(T > T_M)$ , indicating an increase of the magnetic correlations prior to the transition. Up to  $B = 0.5\text{ T}$  the low temperature ( $T < T^*$ )  $C_m(T)$  dependence practically coincide, without affecting substantially the gap of anisotropy nor the  $T^{1.5}$  coefficient determined applying eq.(2), see next section. Since  $C_m(T)$  curves crosses each other (at  $\approx 3\text{ K}$ ), one may conclude that there are degrees of freedom transferred from the intermediate phase (i.e.  $T^* < T < T_M$ ) to the region where dimers form (i.e.  $T > T_M$ ). On the contrary, no degrees of freedom are transferred from  $T < T^*$  by effect of the magnetic field. This indicates that the FM GS is more robust under field than the intermediate phase between  $T_M$  and  $T^*$ .

### III. DISCUSSION

The magnetic nature of the GS can be recognized analyzing the thermal dependence of the specific heat. Below  $T^*$ , the  $C_m(T)$  dependence is properly fitted according to an anisotropic FM relation dispersion like the observed in  $\text{Ce}_2\text{Pd}_2\text{Sn}$  [10]:

$$C_m(T < T^*) = \gamma T + AT^{3/2} \exp(-\Delta_M/T) \quad (2)$$

where  $\gamma$  is the Sommerfeld coefficient and  $\Delta_M$  a gap in the magnon spectrum which rises from zero for  $\text{Pd}(2+y) = 2.2$  up to  $0.4\text{ K}$  for the  $\text{Pd}(2+y) = 2.4$ . Such an increase of  $\Delta_M$  indicates a increasing anisotropy driven by the fact that the Ce-Ce inter-plane distance expands from  $3.963\text{ \AA}$  to  $4.017\text{ \AA}$  [13]. The  $\gamma$  coefficient extracted for these Pd-rich AF alloys is comparable to that of the *La* isotopic compound in agreement with the expected  $\text{Ce}^{3+}$  character of the magnetic ions and the consequent negligible Kondo effect.

For the case of the studied Ce-rich FM alloy  $\text{Ce}_{2.1}\text{Pd}_{1.95}\text{In}_{0.95}$ , a similar thermal dependence is observed, with  $C_m = 0.14 + 4.3T^{3/2} \exp(-2.8/T)$  up to  $T_C$ , see Fig. 6. A FM type dispersion relation is certainly expected because of the spontaneous magnetization observed in  $M(T)$  below  $T_C = 4\text{ K}$ . However, the large  $\gamma = 0.14\text{ J/mol K}^2$  is somehow unexpected from the  $3^+$  character of the Ce atoms and in comparison with that

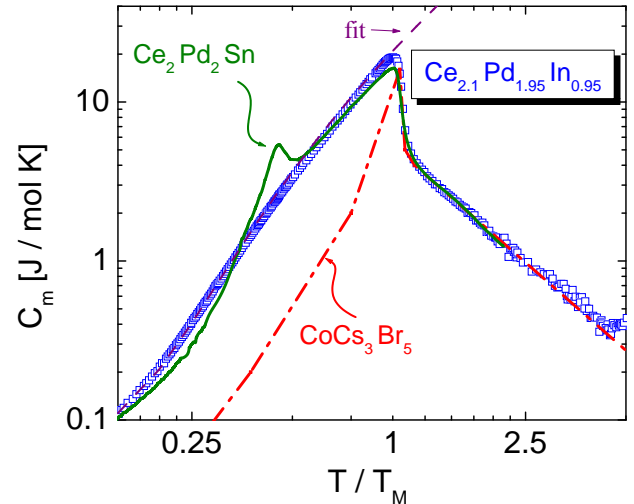


FIG. 6: (Color online) Comparison of the specific heat magnetic contribution of two  $\text{Ce}_2\text{Pd}_2\text{X}$  ( $\text{X}=\text{In}$  and  $\text{Sn}$ ) compounds with the model compound for 2D simple square lattice (dashed dot line), all normalized to their respective ordering temperatures. Dashed curve is the fit to  $\text{Ce}_{2.1}\text{Pd}_{1.95}\text{In}_{0.95}$  using eq(1).

of the AF alloys. This enhanced contribution can be explained by a closer inspection to the interatomic Ce-Ce spacing on the Ce-rich FM-branch provided in Ref. [13]. Although Ce-Ce spacing on plane slightly increases following the 'a' lattice parameter, the situation around the extra Ce atom loci on the  $z = 0$  plane (at the '2a' Wyck-off position) is quite different. Due to the larger atomic radius of Ce atoms with respect to *In* ones, the substituted atoms support a significant 'crystal pressure' which reduces the Ce-Ce spacing below the magnetic limit. As a consequence, hybridization effects may arise between those substituent atoms and their Ce-*nn* on the '4h' position in the  $z = 0$  plane. In such a case, those atoms may contribute to the specific heat as Kondo impurities, increasing the  $\gamma$  coefficient.

Concerning the low temperature properties presented in Fig. 3, there is an apparent contradiction between positive value of  $\theta_P$  expected for a FM system and the AF like cusp in temperature dependence of the susceptibility. Like in  $\text{Ce}_2\text{Pd}_2\text{Sn}$ , this fact indicates that two contributions are competing at that temperature. Both mechanisms are intrinsic to the formation of a ShSu lattice because the FM  $J$  coupling is responsible for the dimers formation above  $T_M$  and the AF  $J'$  couples those dimers to build up the ShSu network below  $T_M$ .



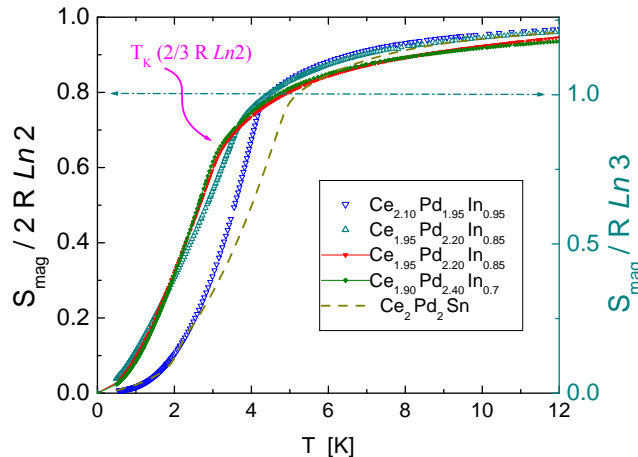


FIG. 7: (Color online) Comparison of the thermal increase of the entropy between indide and stanide compounds.  $T_K \simeq 2/3 R \ln 2$  indicates the curve from which the Kondo temperature is evaluated.

### A. Proving dimers formation

Since the objective of this work is to investigate the effect of electronic (holes) variation on the ShSu lattice stability, the first issue is to ascertain whether dimers actually form in these alloys like in  $\text{Ce}_2\text{Pd}_2\text{Sn}$ . The second is to check whether the magnetic phase below  $T_M$  keeps having the characteristics assigned to ShSu lattices once Sn  $[5s^25p^2]$  is replaced by In  $[5s^25p^1]$  and the number of holes is further increased by  $\text{Pd}$  concentration.

Following the same procedure proposed in Ref.[10] we have evaluated the magnetic entropy gain  $S_{\text{mag}}(T)$  from the measured specific heat as  $S_{\text{mag}} = \int C_m/T dT$ , and included those results in Fig. 7 for different  $\text{Pd}$  concentrations, including one Ce-rich FM alloy. One can see that for the latter compound the 'per Ce atom' entropy at  $T = T_M$  is  $S_{\text{mag}} = 0.8R \ln 2$ , which coincides with the molar entropy of  $R \ln 3$ . Like for stoichiometric  $\text{Ce}_2\text{Pd}_2\text{Sn}$  [10], included in the figure as reference, the formation of FM dimers is inferred. The remaining entropy is collected above the transition since the onset of magnetic correlations occurs at  $T \leq 20$  K as indicated by the  $C_m(T > T_M)$  tail in Fig. 6. Notice that for the  $\text{Ce}_{2.1}\text{Pd}_{1.95}\text{In}_{0.95}$  compound  $C_m(T > T_M)$  nicely coincides with that of the model compound for the 2D-square lattice  $\text{CoCs}_2\text{Br}_5$  [16] and the parent compound  $\text{Ce}_2\text{Pd}_2\text{Sn}$ .

For the alloys belonging to the AF branch, the entropy at  $T_M$  decreases progressively and the criterium to compare  $S_{\text{mag}} = 0.8R \ln 2$  with  $R \ln 3$  can be applied only to the sample close to the stoichiometry, i.e.  $\text{Pd}_{2+y} = 2.2$ . For higher  $\text{Pd}$  concentrations the entropy evaluation has to be normalized to the actual number of

Ce atoms not affected by the proximity of a double  $\text{Pd}$  occupation in sites '4e'. This re-normalization may include the  $\text{Pd}_{2+y} = 2.25$  sample into those where Ce-Ce dimers are formed, but it does not apply satisfactorily to the samples with  $\text{Pd}_{2+y} = 2.35$  and 2.4. Nevertheless, the increase of double occupied '4e' sites progressively destroys the lattice character of the ShSu network.

The value of the Kondo temperature for this system can be evaluated also from the  $S_{\text{mag}}(T)$  results shown in Fig. 7 by applying the Desgranges-Schotte [17] criterion of  $S_{\text{mag}}(T = T_K) \simeq 2/3 R \ln 2$  for a non-ordered system. As shown in Fig. 7  $T_K \approx 3$  K, which is similar to the value found for the parent compound  $\text{Ce}_2\text{Pd}_2\text{Sn}$  [10]. This is one of the lowest values found among the Ce compounds and confirms the  $\text{Ce}^{3+}$  character of this ion.

### B. Proving SSL symptoms

As mentioned in the introduction, one of the characteristic features observed in the exemplary compounds exhibiting a ShSu lattice is the crossing of the  $M(B)$  isotherms at low temperatures. In order to search for this effect in the family of compound under study we have chosen the  $\text{Ce}_{1.95}\text{Pd}_{2.2}\text{In}_{0.85}$  alloy because it shows the more pronounced change of slope of  $M(B)$  within our range of measurement. In Fig. 8 we show the detailed study of those isotherms in the region of temperature between  $1.8 \leq T \leq 3.4$  K. Within the experimental dispersion, one can see that such a crossing occurs between  $2.4 \leq T \leq 3$  K at a field  $B = 0.26 \pm 0.05$  T, where the magnetic moment is  $M = 0.89 \pm 0.01 \mu_B/\text{mol}$ , see the inset in Fig. 8. For higher  $\text{Pd}(2+y) = 2.25$  the crossing occurs at higher field and slightly lower temperature, albeit the slope of the isotherms is not so pronounced and the effect practically vanishes for  $\text{Pd}(2+y) = 2.35$ .

Some thermodynamical consequences can be deduced from the existence of such a crossing. Since within that window of temperature the magnetization does not change, then  $\partial M / \partial T|_B = 0$ , and from Maxwell relations also  $\partial S / \partial B|_T = 0$  is deduced. This implies the existence of an 'isosbestic' point [18], which should be reflected in the corresponding thermodynamic parameters like  $C_m/T(T, B)$ . Effectively specific heat measured at  $B = 0$  and 0.5 T (not shown) cross each other at  $\approx 2.9$  K.

The other characteristic of the SSL is the appearance of quantized  $M(B)$  steps. From the measurements of the  $M(B)$  isotherms no discontinuity was observed probably due to the poly-crystalline nature of the samples. However, the analysis of their derivatives  $\partial M / \partial B|_T$  allows to detect an incipient structure as a function of field as it is shown in Fig. 9. Notice that for that figure we have selected the  $\text{Ce}_{1.95}\text{Pd}_{2.25}\text{In}_{0.8}$  alloy because this effect occurs at the lower limit of temperature  $T = 1.8$  K reached by our magnetometer. Thus, we took profit from the fact that this effect occurs at higher temperature as  $\text{Pd}$  content increases and measured the  $\text{Pd}(2+y) = 2.25$  sample

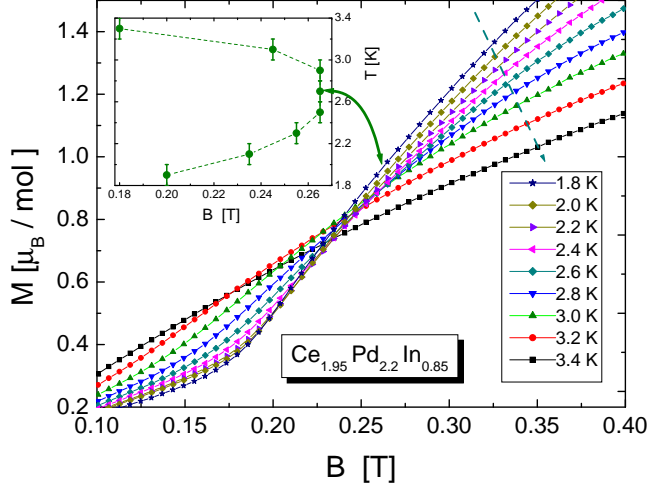


FIG. 8: (Color online) Detail of the  $M$  vs  $B$  isotherms of the  $\text{Ce}_{1.95}\text{Pd}_{2.2}\text{In}_{0.85}$  sample in the region where the crossing occurs. In the inset the temperature and field values of the crossing points are depicted.

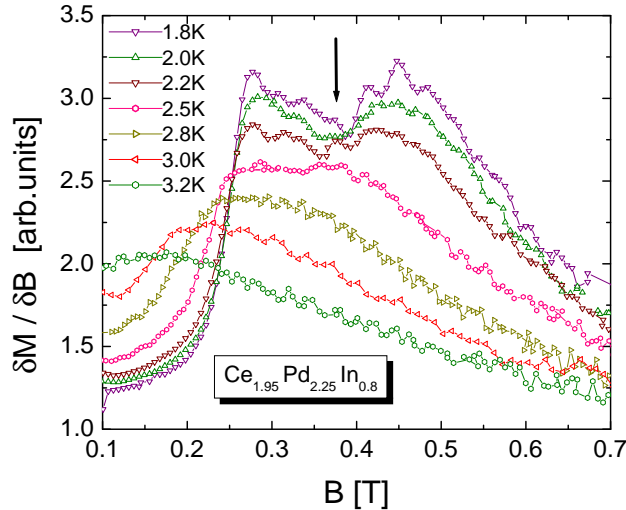


FIG. 9: (Color online) Field dependence of the  $M(B)$  derivative to show the a relative minimum related with an incipient step in  $M$  vs  $B$  isotherms, The arrow indicates the minimum of that derivative which is related with the incipient step.

where at least three isotherms show the mentioned structure in their  $\partial M/\partial B(B)$  dependence. Further increase of  $Pd$ , i.e. for  $Pd(2+y) = 2.35$  and  $2.4$ , strongly weakens the  $M(B)$  curvature smearing out the effect. As shown in Fig. 9 the minimum related with the incipient step occurs at  $B \approx 0.4$  T, where  $M(B) = 0.4 \mu_B$  is  $\approx 1/4 M_{sat}$  since  $M_{sat} \approx 1.3 \mu_B$  [13].

Noteworthy is the comparison between the different fields at which the  $M(B)$  steps occur and the nearly constant temperature of the crossing of  $M$  isotherms for the different mentioned systems. Whereas in  $\text{SrCu}(\text{BO})_3$  the plateaux occur at very high field  $B \approx 20$  T, in metallic  $\text{RB}_4$  it occurs around  $4 < B < 8$  T depending on the crystallographic directions, and at much lower  $B$  (a fraction of Tesla) in  $\text{R}_2\text{T}_2\text{X}$  compounds. In spite of that, the crossing of  $M(B)$  isotherms always occurs at low temperature ( $T < 4$  K). This significant difference between magnetic and thermal scales support the role of the 'quantized magnetization' constrain, making relevant the fact that these effects are related to fractional  $M/M_{sat}$  values. Since in  $\text{SrCu}_2(\text{BO}_3)_2$  a super-exchange mechanism drives the magnetic interactions, high applied field is required to reverse the magnetic nature of the GS in the singlet-triplet level spectrum of the dimers. On the contrary, for RKKY mediated magnetic interactions such a singlet-triplet modification is expected to be much weaker, and consequently lower field would induce the 'quantized magnetization jumps'. On the other hand, the crossing effect depends on relative thermal population of the levels. Once the field driven values for the appropriated  $M/M_{sat}$  values is reached, field independent thermal excitations produce the 'crossing effect'. In other words, this  $M$  vs  $T$  effect cannot be scaled as  $M$  vs  $B/T$ .

### C. Phase Diagram

The magnetic phase diagram as a function of  $Pd$  concentration is shown in Fig. 10a (left side) with  $T_M(Pd)$  defined as the temperature of the maximum value of  $C_m(T)$  and  $T^*(Pd)$  as the temperature of the maximum curvature of  $C_m(T)/T$  defined as a kink for  $Pd(2+y) = 2.20$  and  $2.25$ , and as a 'shoulder' for  $Pd(2+y) = 2.35$  and  $2.40$  in Fig. 1.

This  $y(Pd)$  dependent phase diagram is complemented by the field dependence of the  $Pd(2+y) = 2.4$  sample after an appropriated scaling between  $Pd$  concentration and magnetic field on the right side of Fig. 10b. Although the second order character of the magnetic transition smears progressively out in the  $Pd(2+y) = 2.4$  sample under applied field, the maximum of  $C_m(T, B)$  allows to extend the upper phase boundary up to a magnetic critical point at  $T_{cr} = 2.3$  K and  $B_{cr} = 0.7$  T.

A 3D representation of the magnetic phase diagram is presented in Fig. 11 as a function of both control parameter: field and  $Pd$  concentration, in order to compare the  $B$  dependence of all the AF alloys. In this diagram also one of the Ce-rich FM samples (c.f.  $Pd(2+y) = 1.95$ ) is included with the purpose to test the  $Pd$  concentration (i.e. the 'hole' concentration) as unique parameter able to encompassing the alloys studied in this work, even beyond the gap of miscibility. No further extrapolation on the  $Pd$  dependence can be done within the Ce-rich FM side because in that 'branch' of the phase diagram the free concentration parameter is the  $Ce$  composition,

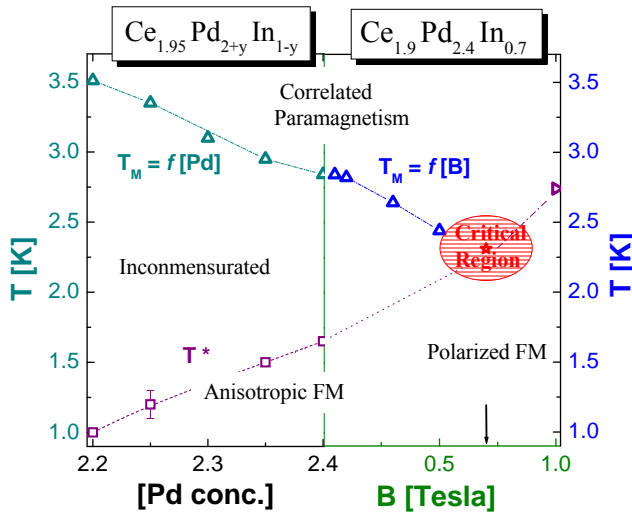


FIG. 10: (Color online) Magnetic Phase diagram as a function of a)  $Pd$  concentration and b) field dependence for the  $Pd_{2.4}$  sample. The arrow indicates the critical field at which the minimum value of  $T_{max}(C_P)$  is observed.

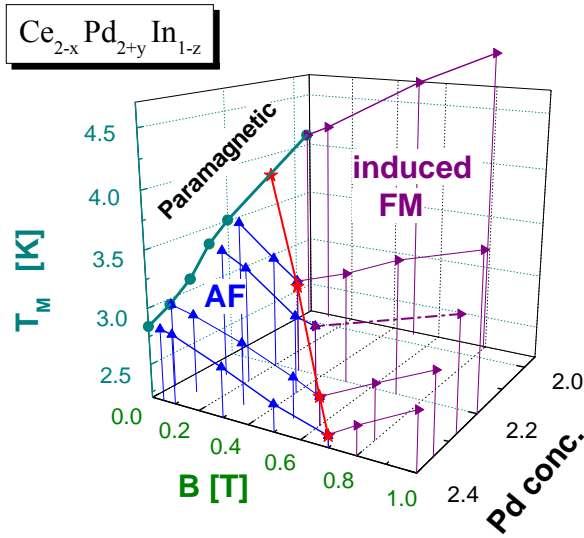


FIG. 11: (Color online) 3D representation of the magnetic phase diagram as a function of  $Pd$  concentration and magnetic field.

whilst the  $Pd$  remains constant [13].

The minima of  $T_M$  as a function of field observed in the AF alloys indicate that the critical field  $B_{cr}(Pd)$ , where the polarized FM behavior takes over, increases with the  $Pd$  content. As expected, the magnetic bound-

ary for  $Pd(2+y) = 2.4$  coincides with the right side of Fig. 10. Notably, the extrapolation of  $B_{cr}(y) \rightarrow 0$  occurs at  $Pd(2+y) = 2.1$ , which lies within the gap between AF and FM branches.

#### IV. CONCLUSIONS

The magnetic properties of the  $Ce_{2-x}Pd_{2+y}In_{1-z}$  family of compounds can be described as a function of a unique parameter: the decrease of the electronic concentration, and consequently their Fermi energy, as the number of 'holes' increase with  $Pd$  concentration.

Their ground state shows a common ferromagnetic character in their magnon dispersion extracted from the specific heat at low temperature. This is confirmed by magnetization measurements. However the transition from their respective paramagnetic states is different depending on the relative  $Ce/Pd$  concentration. The rich  $Ce$  sample shows a typical FM transition. On the contrary, the rich  $Pd$  ones show a transition with AF characteristics which become FM after a characteristic temperature  $T^*$ .

Since the value extracted for the Kondo temperature is extremely low, the magnetic  $4f$  states of the  $Ce$  ions are strongly localized all along the series. Nevertheless, in the  $Ce$  rich sample, the  $Ce$  atoms substituting  $In$  seem to behave differently since their available volume is considerably smaller.

The conditions for a lattice of dimer formation is realized only in the alloys lying closer to stoichiometry, i.e. in the  $Pd(2+y) = 2.20$  and  $2.25$  ones. Higher  $Pd$  concentration distorts the  $Ce$ -lattice inhibiting the formation of a well defined network of those dimers. This reveals the instability of the ShSu lattice with in front of atomic disorder.

Concerning the ShSu phase symptoms in the  $Pd(2+y) = 2.20$  and  $2.25$  alloys, the  $M(B)$  isotherms crossing is observed in the alloys of that AF branch. However, only an incipient modulation in the  $M(B)$  dependence is seen in its derivative. The ploy-crystalline character of this system may explain the weakness of this effect together with its intermetallic nature since the electrons in the conduction band (responsible for the RKKY interaction) are strongly delocalized.

An interesting complement to this research can be to drive the weakening of the  $Ce^{3+}$  moments by chemical pressure.

#### Acknowledgments

This work was partially supported by a CNR (Italy) and CONICET (Argentina) cooperation program, PICTP-2007-0812 and Secyt-UNC 06/C256 projects.

[1] see e.g. C. Lacroix; J. Phys. Soc. Japan **79** 011008 (2010).

[2] B.S. Shastry and B. Sutherland; Physica **108B** 1069



- (1981).
- [3] H. Kageyama, K. Yoshimura, R. Stern, N.V. Mushnikov, K. Onizuka, M. Kato, K. Kosuge, C.P. Slichter, T. Goto, Y. Ueda; Phys. Rev. Lett. **82** 3168 (1999).
  - [4] S. Miyahara and K. Ueda; Phys. Rev. Lett. **82** 3701 (1999).
  - [5] Michimura, 2006 (RB-4)
  - [6] M. S. Kim, M.C. Bennett and M.C. Aronson; Phys. Rev. B **77** 144425 (2008).
  - [7] F. Fourgeot, P. Gravereau, B. Chevalier, T. Roisnel, J. Etorneau; J. Alloys & Comps **238** 102 (1996).
  - [8] M. Giovannini, H. Michor, E. Bauer, G. Hilscher, P. Rogl, R. Ferro; J. Alloys & Comps **280** 26 (1998).
  - [9] M.N. Peron, Y. Kergadallan, J. Rebizant, D. Meyer, S. Zwirner, L. Havela, H. Nakotte, J.C. Sprilet, G.M. Kalvius, E. Colineau, J.L. Oddou, C. Jeandey, J.P. Sanchez; J. Alloys & Comps **201** 203 (1993).
  - [10] J.G. Sereni, M. G.- Berisso, A. Breghta, G. Schmerber and J.P. Kappler, Phys. Rev. B **80** 024428 (2009).
  - [11] J.G. Sereni, M. G.- Berisso, A. Breghta, G. Schmerber and J.P. Kappler, Phys. Rev. B **81** 184429 (2010).
  - [12] J.G. Sereni, J. Phys. Conf. Series, 2010, to be published.
  - [13] M. Giovannini, H. Michor, E. Bauer, G. Hilscher, P. Rogl, T. Bonelli, F. Fauth, P. Fischer, T. Hermannsdorfer, L. Keller, W. Sikora, A. Saccone, R. Ferro, Phys. Rev. B **61** 4044 (2000).
  - [14] J.G. Sereni et al., Phys. Rev. B **75** (2007) 024432.
  - [15] See e.g. M.A. Continentino, S.M. Medeiros, M.T. Otland, M.B. Fontes, E.M.B. Saitovich, Phys. Rev. B **64** 012404 (2001).
  - [16] R.F. Wielinga, H.W. Blöte, J.A. Roest, W.J. Huiskamp, Physica **34** 223 (1967).
  - [17] H.-U. Desgranges and K.D. Schotte, Physics Letters **91A** 240 (1982).
  - [18] M. Eckstein, M. Kollar, D. Vollhardt, J. Low Temp. Phys. **147** 279 (2007).